Minimum energy shapes of one-side-pinned static drops on inclined surfaces

Sumesh P. Thampi and Rama Govindarajan*

Engineering Mechanics Unit, Jawaharlal Nehru Centre for Advanced Scientific Research, Jakkur, Bangalore 560064, India

(Received 17 June 2011; revised manuscript received 2 September 2011; published 10 October 2011)

The shape that a liquid drop will assume when resting statically on a solid surface inclined to the horizontal is studied here in two dimensions. Earlier experimental and numerical studies yield multiple solutions primarily because of inherent differences in surface characteristics. On a solid surface capable of sustaining any amount of hysteresis, we obtain the global, and hence unique, minimum energy shape as a function of equilibrium contact angle, drop volume, and plate inclination. It is shown, in the energy minimization procedure, how the potential energy of this system is dependent on the basis chosen to measure it from, and two realistic bases, front-pinned and back-pinned, are chosen for consideration. This is at variance with previous numerical investigations where both ends of the contact line are pinned. It is found that the free end always assumes Young's equilibrium angle. Using this, simple equations that describe the angles and the maximum volume are then derived. The range of parameters where static drops are possible is presented. We introduce a detailed force balance for this problem and study the role of the wall in supporting the drop. We show that a portion of the wall reaction can oppose gravity while the other portion aids it. This determines the maximum drop volume that can be supported at a given plate inclination. This maximum volume is the least for a vertical wall, and is higher for all other wall inclinations. This study can be extended to three-dimensional drops in a straightforward manner and, even without this, lends itself to experimental verification of several of its predictions.

DOI: 10.1103/PhysRevE.84.046304 PACS number(s): 47.55.D−

I. INTRODUCTION

Understanding how liquid drops remain static on inclined surfaces, despite the action of gravity, is a classical problem. It is not too straightforward to predict the shape attained by such a drop, since a given volume can assume an infinite number of static shapes. Depending on the minute details of the solid surface on which the drop is supported, the contact line adjusts itself so that, microscopically, Young's equation

$$\sigma \cos\theta_e + \sigma_{sl} = \sigma_{sg} \tag{1}$$

is satisfied, thus balancing surface tension forces at the contact line. Here σ, σ_{sl}, and σ_{sg} are the liquid-gas, solid-liquid, and solid-gas interfacial tensions, respectively, and θ_e is the equilibrium contact angle. This microscopic force balance is unaffected by external body forces. However, the observed macroscopic, or apparent, contact angle is often different from θ_e at both the front (θ_f) and the rear (θ_b) of the drop (Fig. 1). The possibility that the microscopic contact angle may be different from the macroscopic is called contact angle hysteresis. A drop on an inhomogeneous solid surface is capable of exhibiting contact angle hysteresis. This phenomenon has been well known experimentally for a very long time, and there are many theoretical studies as well (for example, see Ref. [1]). For a drop on an inclined surface the difference in the apparent contact angles results in a net surface force that balances the gravitational force [2,3]:

$$V\rho g \sin\alpha = k\lambda\sigma(\cos\theta_b - \cos\theta_f), \tag{2}$$

where V, ρ, g, and α are the volume, density of the fluid, acceleration due to gravity, and the plate inclination with respect to the horizontal, respectively, and λ is some characteristic width of the drop. This equation is exact in two dimensions with $k = 1$. However, in three-dimensional drops the value of k is not unique because of the complex shape that a drop may adopt on an inclined surface. Variations in the force related to contact area shape and size, and drop shape, are clubbed together into the factor k in these nonaxisymmetric drops [4,5]. Detailed geometry investigations have been done both experimentally [5,6] and numerically [7,8].

Solids that can support any amount of hysteresis are referred to here as infinitely hysteretic surfaces. Here the small-scale roughness or chemical heterogeneities make it possible for a contact line to shift imperceptibly, in order to microscopically satisfy Young's angle. We distinguish this general property of the surface from that displayed by special locations on the surface where forward motion is prevented; i.e., the contact line is pinned. These are associated with a sharp heterogeneity providing a resistive force too large to be overcome by thermal fluctuations.

In all the numerical investigations we have come across, the shape of the drop is obtained by making some restrictive assumptions such as (1) pinning the contact line to a prespecified shape such as a circle [8] or an elliplse [9], (2) defining a small spherical region somewhere on the interface [7], (3) prescribing apparent contact angles [10], or (4) spherical cap and small hysteresis approximation [11]. Such prescriptions are not unreasonable in certain practical situations, but in the general context they are not valid [12], especially at critical conditions, beyond which surface forces are not able to counter gravity to provide a static shape [13]. Second, some previous studies derived the static shape assuming that it would form the asymptotic static limit of the shape of a moving drop [14–16]. In these studies various experimental observations needed to be made use of, e.g., in Ref. [6] where parallel sided sliding drops were observed, and this was prescribed. Also, a drop on a given surface may display

*rama@jncasr.ac.in

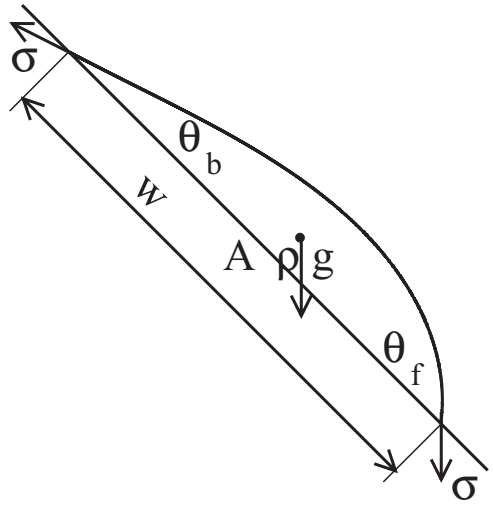

FIG. 1. A static drop on an inclined surface. The weight of the drop is supported by the difference in surface tension forces at the front and rear of the drop.

a particular pair of advancing (θ_a) and receding (θ_r) contact angles in the limit of zero velocity. These, however, need not be the same as the front (θ_f) and back (θ_b) angles it would adopt in its minimum energy configuration [17]. Though some of the results enjoy experimental verification [18], it may be noted that experiments too will not yield unique energy minimum shapes, unless specifically designed to do so. In general there exist a multitude of metastable solutions depending upon the solid characteristics, and a given experiment would lead to only a subset among them.

The idea of considering the resisting force of the solid surface as a gradient of a potential was introduced in Ref. [19]; however, this was not pursued further, since this potential does not have a simple functional form. With the development of new experimental and computational techniques, this problem continues to draw the attention of researchers. An energy minimization procedure for nonaxisymmetric drops based on the principle of virtual displacement has been developed in Refs. [20,21] and a particle-based simulation method in Ref. [22]. While the former introduces resistive forces and hypothesizes a form for it to obtain static shapes, the latter obtains them without explicit use of contact angle hysteresis. A detailed numerical study of the drop geometry leading to an analysis of Eq. (2) is still lacking in the literature. Meanwhile there has been some progress in experimental investigations of various aspects relating shape and surface properties [5,11,12,23,24]. In summary, though some issues have been addressed theoretically [25,26], further studies in theory and numerical simulations are obviously required for a better understanding. We describe here a method to determine the shape, based on minimizing the total energy of the static drop, which does not require experimental input.

There are several situations in which one may ask what is the maximum volume of a drop that can be supported on a solid surface inclined at a certain angle to the horizontal. This question is relevant in various situations, e.g., when insecticides or pesticides are sprayed on plant leaves, in spray and paint industries, or in applications using dropwise condensation heat exchangers. General answers to these questions require a large set of experimental investigations. Our objective here is to make predictions using simple analysis, assuming that the surface is infinitely hysteretic.

Our approach, based on a procedure of minimization of total energy to determine the shape of a static drop, is described in Sec. II. This fundamental approach has been used in several studies [3,10,16,20,21]. The procedure contains one ambiguity, namely, what is the correct base with respect to which the potential energy should be defined. This question has not been addressed explicitly to our knowledge, but different studies get around it by choosing a base and making computations with respect to it. For example, the author of Ref. [3] uses the center of a drop as the base (besides using linearized equations and $\theta_f + \theta_b = 2\theta_e$), those of Refs. [10,16] fix the contact line, while the author of Ref. [21] introduces an artificial resistive force in the procedure for virtual displacements with arbitrary parameters. Each of these choices will give rise to different answers for the minimum-energy shape, and we discuss what would be a good measure under a given situation. Note that the choice of potential energy basis corresponds to a pinning of the drop at a particular point. We deal with one-side pinned situations and hence obtain a more general set of solutions than available in the literature. In fact, a drop pinned on one of its sides and free to choose a minimum energy shape by moving its other end is not uncommon in experiments. The partial pinning of the contact line is a result of variations in solid surface inhomogenities. Experimental investigations in Ref. [27] showed some front-pinned and some rear-pinned drops on inclined surfaces. Rear-pinned drops are generally observed in rain drops on windowpanes; the authors of Ref. [25] investigated this problem experimentally and discussed the partial pinning of the contact line on various surfaces with different affinities. Moreover the phenomenon of hysteresis should be necessarily represented in a correct way to model these drops. But this phenomenon itself is associated with uncertainty, and hence a consistent approach is required. This too has not been discussed to our knowledge and is therefore taken up in Sec. III. Since our approach does not make use of θ_a and θ_r, macroscopic behavior of drops on inclined surfaces such as the the variation of front and rear angles with respect to plate inclination, maximum volume that can be supported on a solid surface at a given inclination, etc., may be addressed consistently.

For simplicity and clarity we analyze two-dimensional drops here, but the method described is general and can be extended to three-dimensional nonaxisymmetric drops. The conclusions of Sec. IV remain valid qualitatively there too. The shapes obtained here may be used as the starting point to study drop dynamics, and to perform stability analyses. Finally, in Sec. V we discuss the future directions and conclude.

II. ENERGY MINIMIZATION

We begin by constructing the force balance on a two-dimensional drop under the action of gravity. We treat the drop as being made up of a liquid (l), in a fluid medium referred to as a gas (g), and supported by a solid surface (s). Since we deal with two-dimensional drops, the term "volume" stands for the cross-sectional area with a unit width in the third (spanwise)

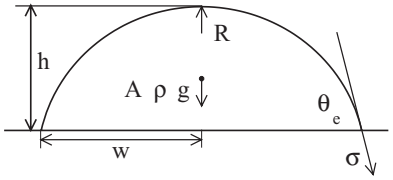

FIG. 2. A sessile drop.

direction. The term "contact area" similarly implies the length of corresponding surfaces times a unit spanwise width.

The hydrostatic pressure variation inside a drop is balanced by a suitable curvature adopted by the flexible liquid-gas interface. For force balance along the vertical (Z) direction, therefore, we must have

$$\frac{\sigma}{R} + z\rho g = \sigma\left\{\frac{d^2z/dx^2}{[1+(dz/dx)^2]^{3/2}}\right\}, \tag{3}$$

where x is the horizontal coordinate at which z is the vertical location of the interface. The term in the fences on the right-hand side is the inverse of the radius of curvature at z, whereas R is the radius of curvature at $z = 0$ (tip of the drop). It is easy to first analyze the two limits, namely, zero plate inclination for a sessile drop and a 180° plate inclination for a pendant drop. Consider a sessile drop, illustrated in Fig. 2, of height h, contact area $2w$ with the solid, and liquid-gas interfacial tension σ, subjected to gravity g. At the contact line, a horizontal force balance yields nothing but Young's equation (1) with the equilibrium contact angle θ_e. The weight of the drop and the vertical component $2\sigma \sin\theta_e$ of the forces due to surface tension are balanced by the reaction from the rigid solid surface [28]. The reaction to the pressure forces is distributed along the contact area, while that to the tension along the interface is a point force at the triple contact point. Thus, an overall vertical force balance for a sessile drop (Fig. 2) can be written [18] as

$$V\rho g = 2w\left(\frac{\sigma}{R} + \rho g h\right) - 2\sigma \sin\theta_e. \tag{4}$$

This expression may also be obtained from the integration of Eq. (3) [29]. Note that surface tension manifests itself both as a point load and a distributed load.

On inverting the plate, we have a pendant drop as shown in Fig. 3, and an overall vertical force balance can be written as

$$V\rho g = -2w\left(\frac{\sigma}{R} - \rho g h\right) + 2\sigma \sin\theta_e. \tag{5}$$

The reversal of the direction of the surface forces results in the shape of pendant drops being different from sessile ones. For a sessile drop, the solid surface can support any weight, but for pendant drops a part of the distributed reaction force acts in the

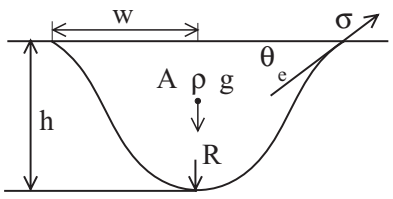

FIG. 3. A pendant drop.

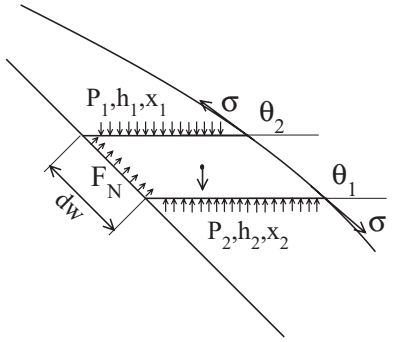

FIG. 4. Forces acting on an elemental volume of drop resting on an inclined surface. The gravitational force is shown acting at the center of gravity of the element; pressure and normal reaction are shown as distributed forces acting over a length while the liquid-gas interfacial tension acts as point force at the two corners.

direction of gravity, and the remainder must support both this and the weight of the drop. Thus drops of volume larger than a particular maximum cannot be "hung" from a solid surface. A detailed discussion specific to pendant drop shapes and their stability can be found in Ref. [30]. We now construct a force balance of a drop sitting on an inclined surface.

The force balance parallel to the solid surface is straightforward. However, the balance in the direction normal to the surface needs some care. A discussion of the normal force balance is not available in the literature to our knowledge, except Refs. [31,32], which discuss the normal reaction force at the contact line alone. Such a discussion is therefore included below. In fact, even for horizontal surfaces, the role of the surface reaction is an important issue drawing recent attention (see, e.g., Refs. [32,33]).

Consider a small element of volume dV shown in Fig. 4 of the drop discussed in Fig. 1. The forces acting on this element are (1) gravitational force $dV\rho g$ acting downward, (2) surface tension forces σ acting at the corners of the liquid-gas interface along the interface, (3) pressure forces Px acting on the upper and lower surfaces of the element, and (4) the reaction force $F_N dw$ from the solid surface. Subscripts 1 and 2 denote the lower and upper faces of this element, respectively. A horizontal force balance of this differential element is given by

$$\left(\frac{\sigma}{R} - \rho g z\right) dw \sin\alpha = \sigma(\cos\theta_1 - \cos\theta_2), \tag{6}$$

where R is the radius of curvature at a point on the interface from where the height z is measured. A vertical force balance is written as

$$\left[\left(\frac{\sigma}{R} - \rho g z_1\right)x_1 - \left(\frac{\sigma}{R} - \rho g z_2\right)x_2\right] + \sigma(\sin\theta_2 - \sin\theta_1) + \left(\frac{\sigma}{R} - \rho g z\right) dw \cos\alpha = dV\rho g. \tag{7}$$

It may be seen that, unlike in sessile and pendant drops, the variation of reaction force along the solid surface is not intuitively obvious. For example, the nontrivial geometry (say, $x_1 \neq x_2$) gives rise to several contributions. Integrating the

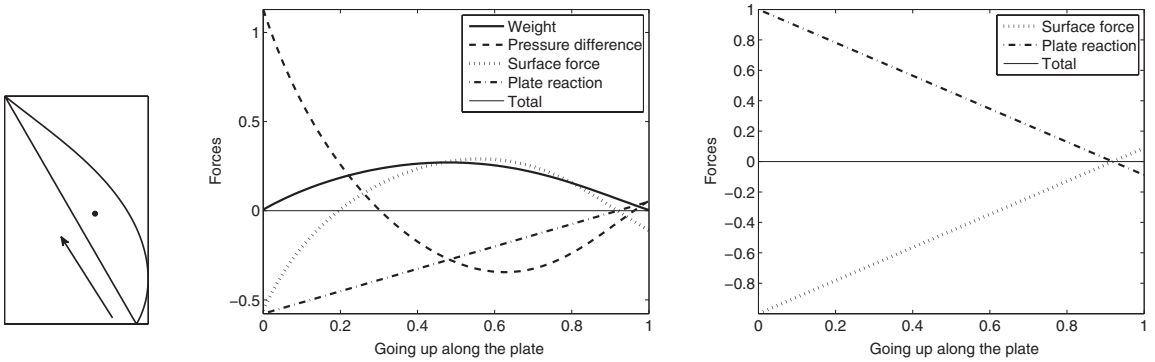

(a) Drop shape (b) Vertical force balance (c) Horizontal force balance

FIG. 5. Distribution of forces acting on the drop along the plate, resolved into vertical (b) and horizontal (c) components for the shape shown in (a). $z = 0$ on the abscissa corresponds to the front end of the drop. Forces are normalized on the ordinate. In (a) and in subsequent figures, the center of mass is shown by a point.

horizontal and vertical force balances on such elements for the entire drop volume, and resolving the total force in a direction parallel to the plate, Eq. (2) may be recovered. Correspondingly the total force balance in a direction normal to the plate is

$$V\rho g\cos\alpha + \sigma(\sin\theta_f + \sin\theta_b) = \frac{1}{\sin\alpha}\left\{\frac{\sigma}{R}(h_r - h_a) - \frac{\rho g}{2}\left[h_r^2 - h_a^2\right)\right\}, \qquad (8)$$

where h_r and h_a denote the height to the locations of rear and front contact points from where R is defined. This expression reduces to Eqs. (4) and (5), respectively, when plate inclination goes to 0° and 180°.

To understand the relative distribution of these forces, we plot them in Fig. 5. We consider a typical shape as shown in Fig. 5(a). The force contributions along the vertical and horizontal directions are shown in the Figs. 5(b) and 5(c), respectively. In fact, the reaction force changes direction at a particular height. Thus the bottom part of the drop is supported by the solid while the top is not. It is obvious that the solid wall should provide the necessary local moment reaction as well, since the lines of action of the various forces do not coincide. Therefore the drop cannot be thought of as *pivoted* at a single point on the plate, unlike a solid object hanging from a point.

III. NUMERICAL METHOD OF DETERMINING THE SHAPE

The procedure used is an extension to inclined surfaces of that described in Ref. [30] for pendant drops. Beginning with a specified value of R, Eq. (3) is integrated to determine a possible equilibrium shape of the meniscus. Note that this equation is independent of the positioning of the solid plate. Using this freedom, the solid plate at a specified inclination is used to cut this curve when the volume of the closed shape corresponds to the desired volume V. For this fixed volume, the result corresponds to a unique force-balanced shape for the specified bottom-most radius of curvature R. Figure 6 illustrates shapes so obtained, of a given volume on a particular plate inclination for two different values of R. In principle, an infinite number of such shapes can exist in nature for a given volume.

Given an infinitely hysteretic solid, the shape that will actually be displayed will be the minimum energy one for the given combination of solid surface and fluid. Our objective is to find that unique shape at which the drop attains the least energy it possibly can, on all possible surfaces of a given surface tension. The total surface energy (E_s) may be calculated as

$$E_s = \sigma L_{lg} + (\sigma_{sl} - \sigma_{sg})L_{sl}, \qquad (9)$$

where L_{lg} and L_{sl} are the liquid-gas and solid-liquid interfacial lengths. The quantity that needs care in defining is the total potential energy (E_p), which may be written as

$$E_p = V\rho g(h_{cg} - h_{\text{ref}}), \qquad (10)$$

where h_{cg} is the height of the center of gravity of the drop. There is an arbitrariness in choosing the reference height h_{ref}, and evidently the results depend crucially on this choice. For example, one may take h_{ref} as the point on the plate vertically below the center of gravity. The rear or front contact line locations, and also the midpoint on the contact length, present

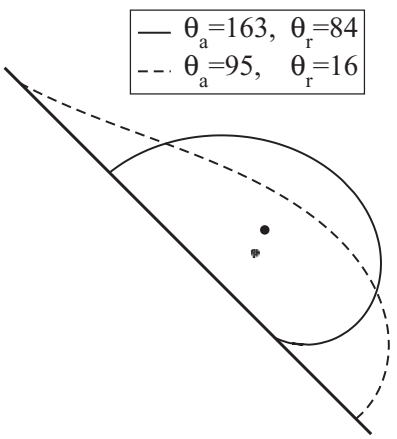

FIG. 6. Illustrating two different shapes for the same volume and plate inclination, corresponding to two different values of R. Both shapes are possible to achieve in experiments by choosing solid surfaces of appropriate characteristics.

other natural choices. The physical basis for a particular choice is open to question. This problem of determining the right base for the calculation of potential energy is not very common in mechanics. It is usual that the choice of basis changes the potential energy only by a constant value in all cases, which does not matter in any comparisons. Here we have a peculiar situation in which a deformable body with free end points is allowed to slide on an inclined surface. In theory the drop as a whole may be translated to lower and lower positions on the solid surface, and its total energy would keep decreasing. In the case of a solid object hanging from a wall, there would be a well-defined pivot point of suspension from the wall. There is no such unique point for a liquid drop as we have discussed. The reason the drop attains an equilibrium position in reality is because of pinning of some kind at one or more contact locations. The most reasonable choices for h_{ref} are thus either the advancing or the receding fronts of the drop, and we study both. We also do cross-comparisons between these choices. As discussed in Sec. I, the more restrictive situation where both ends are pinned is well studied in the literature. That case, however, involves an arbitrary choice of contact line length. In reality when a drop slides on an inclined surface, its movement is restricted typically by the pinning of just one of its ends.

Not all boundary conditions are known *a priori* in this free boundary value problem and are to be determined along with the full solution. Such a procedure is straightforward for droplets on a horizontal surface, where Young's equation arises naturally from the energy minimization process. One may apply a similar procedure for drops on inclined surfaces. In this case, the energy minimization procedure not only arrives at Eq. (2) as the boundary condition, but picks a unique combination of θ_f and θ_b. It is thus more powerful than earlier procedures, which needed to provide an additional prescription, e.g., of contact angle or contact area. More important, we have the global minimum energy shape rather than innumerable metastable solutions. A drop on an inclined surface would remain in motion until it encounters a pinning location. At the pinning location, the surface provides a restraining force, which is far stronger than the thermal fluctuations can overcome. This strong force could come from a sharp chemical heterogeneity, for example. It is reasonable to assume that such pinning is likely to occur at one end of the drop [25,27], and that both ends are unlikely to be pinned simultaneously. A choice of pinning location fixes the basis for potential energy calculations. At the free end, thermal fluctuations allow the contact line to relocate itself at small scales to minimize energy. We emphasize again our assumption that the solid surface is capable of exhibiting the full range of front and back contact angles, and that enough thermal energy is available to the drop to take up the most stable shape at the free end. This concept is pictorially represented in Fig. 7. The left portion of the figure shows a case where there is no minimum energy static shape, so the drop will continue to move downward on the incline. This would happen when the drop is larger than the maximum permissible static volume, for example. On the right we have a possible energy minimum shape. We also need an appropriately placed pinning location, as discussed. This pinning on one side gives a general set of solutions unlike the solutions obtained in the literature with the entire contact area pinned.

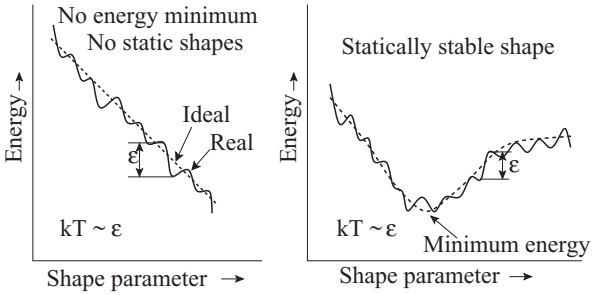

FIG. 7. Example schematics of energy landscapes. The total energy for an ideal (dashed lines) and real (solid lines) solid surface is shown as a function of some continuous variation in drop shape characteristics. Local heterogeneities produce local minima of depth $O(\varepsilon)$, and kT is the thermal energy available to the system. Our procedure essentially looks for a global energy minimum of the type illustrated in the right schematic. The location of pinning provides an additional strong restraining force that is too strong for thermal fluctuations to overcome. In a landscape of the form shown on the left, our procedure will not yield a static shape.

The total energy may be written as the sum of potential and surface energies, $E_t = E_p + E_s$. Substituting Eq. (9) and (10) and nondimensionalizing length scales by capillary length $L_c = \sqrt{\sigma/(\rho g)}$ and energy by σL_c we have the expression for total energy $E_t = B(h_{cg} - h_{\text{ref}}) + L_{lg} - \cos\theta_e L_{sl}$. Here $B = V\rho g/\sigma$ is the Bond number describing the relative importance of two competing forces. We note that other forces which may become relevant in a given situation may be incorporated into the present procedure. It should be mentioned that energy contributions from small unevennesses in the surface are neglected in these calculations, as are other molecular forces.

IV. RESULTS AND DISCUSSION

A. Shape variations

The change in the minimum-energy shape of a drop of a given volume, when the solid surface is tilted in stages from $\alpha = 0^\circ$ to 180°, is illustrated in Fig. 8. It is seen that the shapes corresponding to front-pinned and rear-pinned drops can be dramatically different, highlighting the important role of solid surface heterogeneities. There is no such ambiguity, of course, for sessile or pendant drops. There is a continuous variation

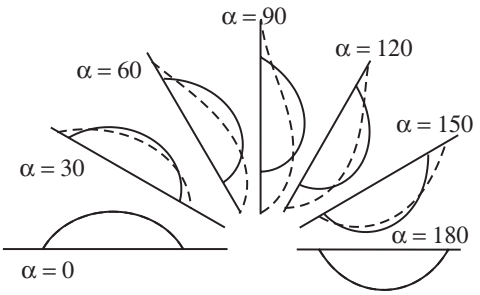

FIG. 8. Illustration of change of global minimum energy shape as a function of plate inclination. Here $\theta_e = 60^\circ$ and $V = 0.5$. Continuous and dashed lines are for shapes obtained by pinning the front and rear of the drop, respectively. It may be noticed that the free end always reaches the equilibrium contact angle.

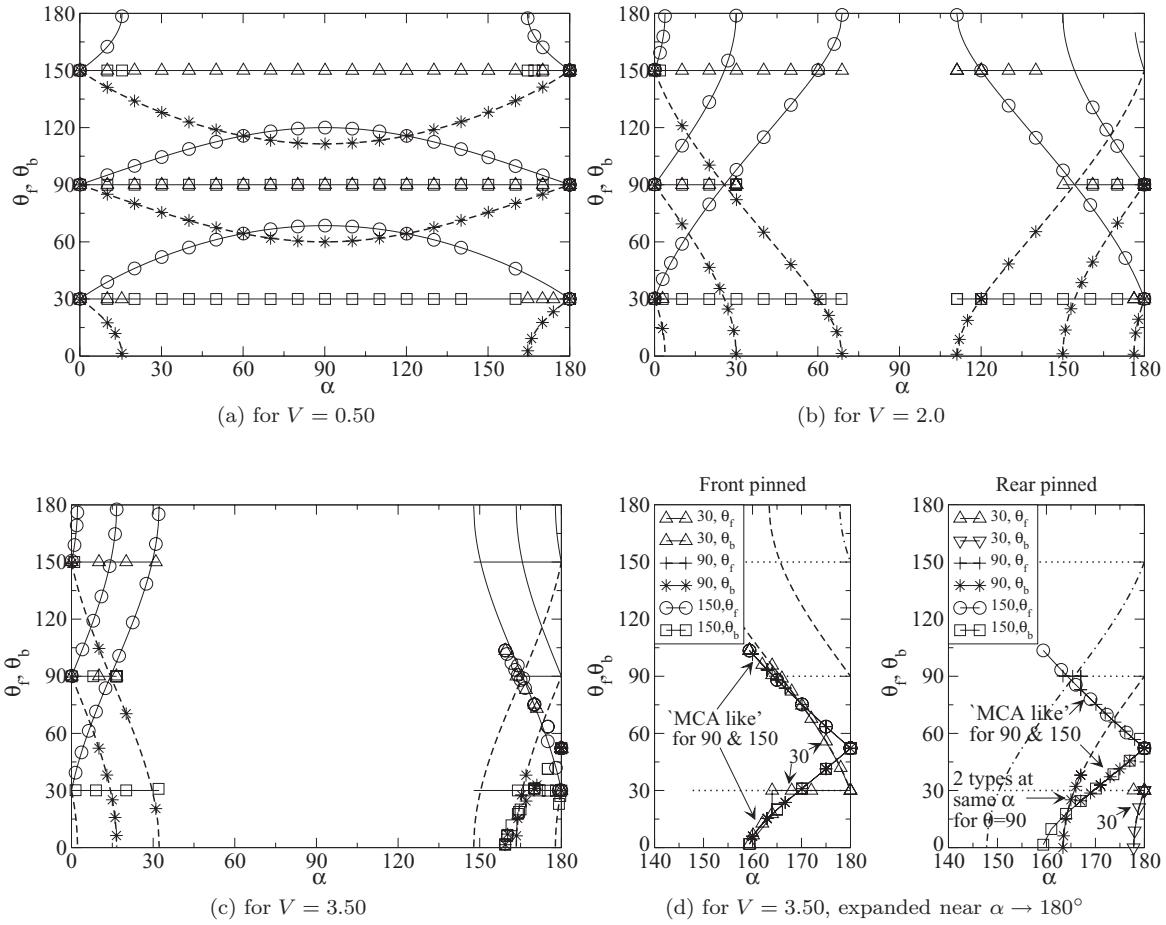

(a) for $V = 0.50$ (b) for $V = 2.0$

(c) for $V = 3.50$ (d) for $V = 3.50$, expanded near $\alpha \to 180^\circ$

FIG. 9. Front and rear contact angles of minimum energy shapes are shown as functions plate tilt angle in (a), (b), and (c) for different volumes of the drop. Three different equilibrium contact angles, $\theta_e = 30^\circ$, 90°, and 150° are considered for each volume. Always $\theta_f > \theta_r$. The computational results are shown with symbols. Solid lines and dashed lines are the theoretical predictions of Eq. (11) for front-pinned and back-pinned drop shapes, respectively. When the front is pinned, the front and back contact angles are represented by $\circ$ and $\square$, respectively. In the case of back pinned, they are, respectively, represented by $\diamond$ and $*$. For a range of inclinations, solutions may not exist, and this is accentuated at larger volumes as in (b) and (c). In (d) a portion of Fig. 9(c) is expanded, to show the existence of different types of solution when $\alpha \to 180^\circ$ for both front-pinned and rear-pinned cases. The symbols for this plot are defined in the legend.

in the contact angle as a function of the tilt angle, with a reversal in behavior at the vertical position of the plate. This is illustrated in Fig. 9.

Figure 9(a) shows the variation in front and rear contact angle as a function of tilt for a nondimensional volume of $V = 0.5$. The plots are done for three different equilibrium contact angles $\theta_e = 30^\circ, 90^\circ$, and 150°. It is seen that the variation in θ_f and θ_b is not symmetric and depends on which side of the drop is pinned. First, consider the case of $\theta_e = 90^\circ$. For a drop pinned at its front, θ_f increases with tilt for $\alpha < 90^\circ$, while the rear adjusts itself to attain $\theta_b = \theta_e$. The opposite happens when the receding side is pinned, in which case the advancing front takes up the most favored contact angle, i.e., θ_e, while the rear angle is forced to reduce. The maximum difference in the two contact angles is seen at the vertical position of the plate, with a monotonic and symmetric variation on either side, to θ_e at the sessile and pendant limits.

For $\theta_e = 30^\circ$, when the front is pinned, the variation is similar to what is observed in the case of $\theta_e = 90^\circ$. But when the back is pinned, there is a sharp decrease in the contact angle, reaching a value of 0° at an $\alpha = 15.5^\circ$, with no solutions beyond, up to $\alpha = 164.5^\circ$. Conversely for $\theta_e = 150^\circ$, when the back is pinned, solutions exist for all inclinations, while there is a large range of α where no solution exists when the advancing front is pinned. There is thus a cross symmetry in the solutions of $\theta_e = \beta^\circ$ and $\theta_e = (180 - \beta)^\circ$, seen for a range of β.

The important observation is that the contact angle at the free end remains at the equilibrium value except for a class of solutions discussed later. For a front-pinned drop, then, $\theta_b = \theta_e$ and $\theta_f > \theta_b$, while $\theta_f = \theta_e$ and $\theta_b < \theta_f$ for a drop pinned on receding side. A use of this information reduces an unknown in Eq. (2), making it solvable. The angle at the pinned end can then be described by

$$\cos\theta_{f/b} = \cos\theta_e \mp V \sin\alpha. \tag{11}$$

Solutions of this equation are plotted as lines in Fig. 9 and are identical to the numerical solutions over most of the range. In experiment, depending on the surface properties, the free end may exhibit an angle lying between θ_r and θ_a, but different from θ_e. Nevertheless, this angle will remain constant for the

given surface irrespective of the inclination and volume. This feature of minimum energy shapes has been seen, but not commented upon, in experiments [2].

The discussion above was for a case when a drop is pinned at one of its ends. Consider now a drop that is effectively pinned elsewhere or has a more complicated distribution of pinning. Many experimental observations show a simultaneous variation in the front and rear angles [23], which is characteristic of such pinning. In our simulations, with the drop pinned elsewhere we observed such a variation of θ_f and θ_b. We also found that for this situation we obtained equal deviations in front and back angles from the Young angle, i.e., $\theta_f = \theta_e + \epsilon$ and $\theta_b = \theta_e - \epsilon$. For small ϵ, the force balance parallel to the plate Eq. (2) then provides

$$V \frac{\sin\alpha}{\sin\theta_e} = \epsilon. \tag{12}$$

With an increase in the volume, as illustrated in Figs. 9(b) for $V = 2.0$ and 9(c) for $V = 3.5$, there is a wider range of tilt angles at which no solution is possible. The symmetry about $\alpha = 90^\circ$ is seen here too. Equation (11) predicts drop shapes over a larger range than that in which numerical shapes are found, especially for higher Young angle and higher α. This is because certain shapes have intersecting menisci and cannot be considered as physical solutions. This was pointed out in Ref. [30] for pendant drops. Since Eq. (11) does not care about this intersection of menisci, it predicts solutions in this range.

There is a crowding of solutions near $\theta_e = 30^\circ$ in Fig. 9(c) when α is close to 180°. This region is expanded in Fig. 9(d) for both front pinned and rear pinned drops. This crowding is related to a subtle point described in detail in Ref. [30]. For a pendant drop, there exists a maximum volume beyond which solutions respecting Young's contact angle do not exist [29]. However, certain solutions, with contact angle smaller than θ_e, may be found beyond this maximum volume, up to $V \approx 5.2$, which is the maximum volume for a fully wetting pendant drop. These solutions are characterized by a local minimum in contact area (MCA). This is seen in Fig. 9(c) with larger volumes exhibiting small contact angles when $\alpha = 180^\circ$. Remnants of these solutions may be found for surfaces inclined at α close to 180° too, and we call them "MCA-like" solutions. These shapes will need further investigation for a full understanding, as discussed in Ref. [30], and we do not pursue that here.

B. Maximum volume

The previous observations lead to Fig. 10 where the maximum volume that can be supported by a plate is plotted against the plate inclination. Again a prediction for maximum volume may be made from Eq. (11), rewritten as

$$V_{\max} = \frac{\cos\theta_e \mp \cos\theta_{f/b}}{\sin\alpha}, \tag{13}$$

where $\theta_f = 180^\circ$ for a front-pinned drop and $\theta_b = 0^\circ$ for a rear-pinned drop. This is shown as a dashed line in the same figure. Note that by substituting Eq. (2) into the expression of Ref. [15] for maximum volume [Eq. (5.3) in that paper] results in this critical volume becoming independent of plate inclination and dependent only on θ_a. Equation (13) would thus provide a more reliable estimate for inclined geometries.

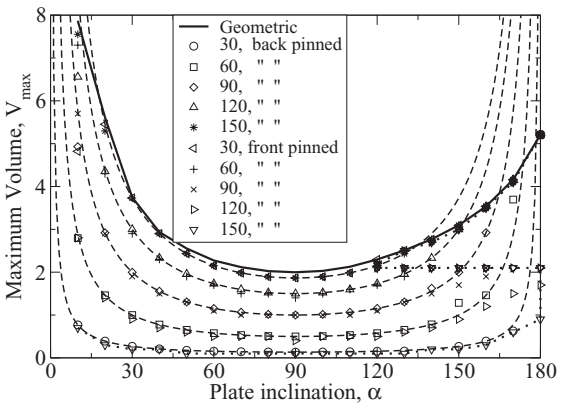

FIG. 10. Maximum volume of a two-dimensional drop that can be sustained on an inclined plate, as a function of inclination. There is a geometrical constraint shown by the dark continuous line. Different dashed lines are predictions of Eq. (13), and symbols are obtained from the numerical calculations for various equilibrium contact angles. A similarity between θ_e of front-pinned and $180^\circ - \theta_e$ and back-pinned is evident.

In fact, a special form of Eq. (13) for hydrophilic surfaces when the receding side forms a thin film, but for three-dimensional drops, has been reported in Ref. [25] and experimentally verified. This particular case corresponds to a drop pinned at the back, with $\theta_b \sim 0^\circ$, and hence Eq. (13) conforms to Eq. (6) of Ref. [25]. Second, we recall that the maximum volume at a given inclination for a particular θ_e when advancing front is pinned coincides with solution for $180^\circ - \theta_e$ when receding side is pinned and vice versa. This may be seen to be a consequence of Eq. (13).

There is another, geometrical, measure of maximum volume. This corresponds to a static drop shape but need not be a minimum energy shape, and is obtained merely by fixing the front angle to 180° and/or the rear angle to 0°. (It may not be possible always to satisfy both due to geometrical reasons.) This is shown by a continuous line. This geometrically achievable maximum need not in general correspond to a minimum in energy, so the true maximum would often be smaller, as seen. Since volume goes to infinity for sessile drops it was difficult to get accurate answers numerically for small plate inclinations.

There are some features to be noticed. Unlike the contact angles, the maximum volume is not symmetric with respect to the vertical position of the plate. The behavior seen is in qualitative agreement with experimental observations of Ref. [18] and theoretical predications of Refs. [14,15] for three-dimensional nonaxisymmetric drops. The asymmetry is to be expected because, as discussed, the plate cannot support an infinite volume in the pendant configuration, but it can in the sessile one, since the plate reaction is finite in the pendant case. At some critical value $\alpha_{\rm cr}$ of the inclination, the normal reaction becomes the limiting factor for maximum volume that can be supported, and Eq. (13) is no longer the decisive equation. In other words, Eq. (9) is the determining condition when $\alpha \to 180^\circ$. This equation is not completely predictive unlike the force balance parallel to the plate due to several unknowns and the interface shape has to be solved to use this equation. This transition of dominant force balance

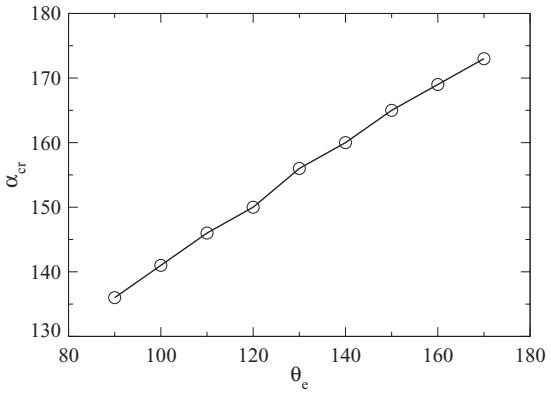

FIG. 11. Critical inclination, beyond Eq. (13) is no longer the decisive condition, as a function of equilibrium contact angle when the front end is pinned.

is important in practical cases because it is not possible to achieve a static shape beyond this critical volume by adjusting fluid or solid properties. The critical inclination of transition, beyond which Eq. (13) is not the decisive condition, is found to vary linearly with equilibrium contact angle as shown in Fig. 11.

Similar to Eq. (13), the expression for maximum volume for a three-dimensional drop can be written as

$$V_{\max} = k\lambda \frac{\cos\theta_e \mp \cos\theta_{f/b}}{\sin\alpha}, \tag{14}$$

where $\theta_f = 180^\circ$ for a front pinned drop and $\theta_b = 0^\circ$ for rear-pinned drop.

In brief, a solid-philic drop has maximum volume when it is front pinned, and a solid-phobic drop has maximum volume when it is back pinned. Our observations tell us how to manipulate solid and fluid properties to support a large volume on a solid surface. For example, by making $\theta_a - \theta_e$ larger one may be able to pin the drop at the front more easily to hold a large volume without falling off. In contrast it may be desirable to keep $\theta_e - \theta_r$ large to hold a solid-phobic drop on an inclined plate.

V. SUMMARY AND OUTLOOK

Static two-dimensional drops on inclined surfaces are studied using a one-dimensional energy minimization procedure, which determines the unique, global energy minimum shapes for a given volume and plate inclination. The contact line length and contact angles of this static drop shape emerge out of the solution procedure and are not fixed *a priori* unlike in earlier studies.

The solution depends on the basis chosen for potential energy. This is discussed, and pinning at the front end and the back end of the drop are chosen as two most realistic measures for freely sitting drops on inclined surfaces. The free end of the drop then attains Young's contact angle, while the angle at the pinned end adjusts itself to minimize the total energy. For any other choice of basis for potential energy calculation, both front and rear angles change simultaneously in equal magnitudes but in opposite sense. The angles subtended at the two ends for minimum energy are thus unrelated to the zero-velocity limit of the advancing and receding contact angles on a surface. The range of parameters over which solutions are possible are delineated.

A detailed force balance is carried out for the first time to our knowledge. It emerges that the reaction force of the solid surface can be of opposite signs over different portions of the contact area, and the plate can thus aid and oppose gravity over different portions. This determines the maximum volume that the plate can support at a given inclination. It is seen that this maximum volume is the least when the plate is held vertical. Below a critical inclination α_{cr} for a given θ_e, the maximum volume varies symmetrically with respect to plate inclination about the vertical, and may be described by Eq. (13). Inclinations α larger than this angle, however can support only a smaller drop volume than inclinations of $180^\circ - \alpha$.

This study may now be extended in several directions, the obvious one being to three dimensional nonaxisymmetric drops. Many of these observations may be verified through experiments on a surface which permits large hysteresis. Another interesting experimental possibility is to obtain both the distributed load and the point forces on the surface, for example, by using a soft material with measurable deformation, and compare against the force balance study here. Apart from this, these minimum energy two-dimensional shapes may be subjected to stability analyses. Though there exist a large literature on the stability of sessile and pendant drops, such studies on inclined drops are fewer.

[1] J. F. Joanny and P. G. de Gennes, J. Chem. Phys. **81**, 552 (1984).
[2] G. Macdougall and C. Ockrent, Proc. R. Soc. London A **180**, 151 (1942).
[3] Y. I. Frenkel, J. Exptl. Theoret. Phys. (USSR) **18**, 659 (1948).
[4] K. Kawasaki, J. Colloid Sci. **15**, 402 (1960).
[5] A. I. El Sherbini and A. M. Jacobi, J. Colloid Interf. Sci. **273**, 556 (2004).
[6] J. J. Bikerman, J. Colloid Sci. **5**, 349 (1950).
[7] B. K. Larkin, J. Colloid Interf. Sci. **23**, 305 (1965).
[8] R. A. Brown, F. M. Orr Jr., and L. E. Scriven, J. Colloid. Interf. Sci. **73**, 76 (1980).
[9] A. Lawal and R. A. Brown, J. Colloid Interf. Sci. **89**, 346 (1982).
[10] H. Merte Jr. and S. Son, Warme Stoffübertrag **21**, 163 (1987).
[11] D. Quere, M. J. Azzopardi, and L. Delattre, Langmuir **14**, 2213 (1998).
[12] C. W. Extrand and Y. Kumagai, J. Colloid Interf. Sci. **170**, 515 (1995).
[13] F. Milinazzo and M. Shinbrot, J. Colloid Interf. Sci. **121**, 254 (1987).
[14] E. B. Dussan and R. T. Chow, J. Fluid Mech. **137**, 1 (1983).
[15] E. B. Dussan, J. Fluid Mech. **151**, 1 (1985).

[16] Y. Rotenberg, L. Boruvka, and A. W. Neumann, J. Colloid Interf. Sci. **102**, 424 (1984).
[17] B. Krasovitski and A. Marmur, Langmuir **21**, 3881 (2005).
[18] B. J. Briscoe and K. P. Galvin, Colloid Surface **52**, 219 (1991).
[19] R. Finn and M. Shinbrot, Math. Method Appl. Sci. **10**, 165 (1988).
[20] S. D. Iliev, Comput. Methods Appl. Mech. Eng. **126**, 251 (1995).
[21] S. D. Iliev, J. Colloid Interf. Sci. **194**, 287 (1997).
[22] A. K. Das and P. K. Das, Langmuir **25**, 11459 (2009).
[23] A. I. El Sherbini and A. M. Jacobi, J. Colloid Interf. Sci. **299**, 841 (2006).
[24] P. S. Yadav, P. Bahadur, R. Tadmor, K. Chaurasia, and A. Leh, Langmuir **24**, 3181 (2008).
[25] P. Roura and J. Fort, Phys. Rev. E **64**, 011601 (2001).
[26] A. I. El Sherbini and A. M. Jacobi, J. Colloid Interf. Sci. **273**, 566 (2004).
[27] V. Berejnov and R. E. Thorne, Phys. Rev. E **75**, 066308 (2007).
[28] P. G. de Gennes, F. Brochard-Wyart, and D. Quere, *Capillarity and Wetting Phenomena: Drops, Bubbles, Pearls, Waves* (Springer, New York, 2004).
[29] E. Pitts, J. Fluid Mech. **59**, 753 (1973).
[30] P. T. Sumesh and R. Govindarajan, J. Chem. Phys **133**, 144707 (2010).
[31] R. Tadmor, K. Chaurasia, P. S. Yadav, A. Leh, P. Bahadur, L. Dang, and W. R. Hoffer, Langmuir **24**, 9370 (2008).
[32] E. R. Jerison, Y. Xu, L. A. Wilen, and E. R. Dufresne, Phys. Rev. Lett. **106**, 186103 (2011).
[33] R. Finn, Phys. Fluids **18**, 04710 (2006).